International Journal of Heat and Mass Transfer 52 (2009) 3585–3594

Contents lists available at ScienceDirect

International Journal of Heat and Mass Transfer

journal homepage: www.elsevier.com/locate/ijhmt

Three-dimensional polymer melt flow in sudden expansions: Non-isothermal flow topology

P.S.B. Zdanski *, M. Vaz Jr.

Department of Mechanical Engineering, State University of Santa Catarina, Campus Universitário Prof. Avelino Marcante, Joinville-SC 89223-100, Brazil

ARTICLE INFO

Article history:
Received 13 November 2008
Received in revised form 12 March 2009
Accepted 12 March 2009
Available online 17 April 2009

Keywords:
Non-Newtonian flow
Viscous heating
Three-dimensional sudden expansion
Numerical simulation

ABSTRACT

Three-dimensional, non-isothermal, polymer melt flow in sudden expansion is numerically investigated. The main goal of the paper is to study the general features of the flow field. The generalized Newtonian formulation is adopted, and the mathematical model corresponds to the laminar, incompressible Navier–Stokes equations. A second order finite difference scheme is used to discretize the governing equations in a collocated mesh. The non-Newtonian flow behaviour is modelled by the Cross constitutive relation, in which temperature effects are accounted for. The simulations show that, despite the high viscosity exhibited by polymer melts, a complex three-dimensional flow structure is found close to the expansion section, characterized by a spiral motion. The results also indicate that viscous dissipation causes limited effect in temperature rise and viscosity variations. The latter was found mostly affected by the shear rate.

1. Introduction

Polymer melt flow in sudden expansions is frequently found in industrial operations such as injection moulding. Along with its interest as a benchmark problem for testing numerical schemes, this flow geometry has instigated researchers on understanding new physical aspects of the flow dynamics. The available literature data is mainly devoted to 2D analysis and there is relatively little information on three-dimensional flows. In addition, most works adopt an isothermal approach, thereby precluding the influences of the mould and injection temperatures and analysis of the viscous heating (caused by the high fluid viscosity), amongst other thermal effects. Therefore, this study aims at elucidating the complex flow pattern exhibited by the non-isothermal 3D flow in plane asymmetric sudden expansions. The paper discusses typical results for this class of coupled and nonlinear problems such as recirculation and vortical characteristics, temperature and viscosity distributions. Markedly, the nonlinear character of the material constitutive relation and the thermally dependent viscous behaviour contrast with similar studies available in the literature for Newtonian fluids, mostly air flow.

Fluid flow in sudden expansions is characterized by the existence of recirculation regions and steep properties variations, being a challenge for any numerical scheme. The literature shows many recent works on the analysis of 2D power-law fluids in sudden expansions, most of which dealing with hydrodynamic instabilities (bifurcation) that may occur at some critical Reynolds number [1–4]. In this case, bifurcation is said to occur when a transition from a symmetric to an asymmetric flow topology in symmetrical sudden expansions takes place. Pinho et al. [5] presented a study on pressure losses and reattachment length for the laminar power-law, non-Newtonian flows in 2D sudden expansions. The authors addressed the influences of the power-law index on such flow parameters. Issues related to pressure losses in contraction/expansion flows were also discussed by Binding et al. [6] using the Oldroyd-B fluid model to describe the non-Newtonian flow behaviour. Interestingly, most works are focused on applications using relatively large Reynolds numbers, which are typical of polymeric solutions or other non-Newtonian fluids, but exceedingly high for polymer melts.

Two-dimensional sudden expansions were also adopted by Bao [7] and Vaz Jr. and Zdanski [8] to validate their numerical schemes (finite elements and finite differences, respectively). Both works used the generalised Newtonian approach and were able to capture the same steady-state flow topology, i.e., a confined recirculation region at the concave corner. Furthermore, a control volume/finite element method was employed by Chen and Hsu [9], where the unsteady polymer melt flow in the mold filing stage is simulated. It is worth mentioning that all aforementioned works, except for reference [8], considered isothermal flow field. Wachs et al. [10] presented an interesting study on the thermal effects in 2D contraction flows. The authors compared isothermal and non-isothermal flow solutions and discussed some important issues regarding distinct constitutive models. Considerations on the thermal effects (including viscous heating), influences of the expansion ratio on

* Corresponding author. Tel.: +55 47 40097971; fax: +55 47 4009 7940.
E-mail address: zdanski@joinville.udesc.br (P.S.B. Zdanski).

0017-9310/$ - see front matter © 2009 Elsevier Ltd. All rights reserved.
doi:10.1016/j.ijheatmasstransfer.2009.03.004

Nomenclature

A	channel cross section $A = W \times H$ (m^2)
AR	aspect ratio $AR = W/S$
c	specific heat (J/kgK)
ER	expansion ratio $ER = H/h$
h	channel thickness upstream of the expansion section (m)
H	channel thickness downstream of the expansion section (m)
k	thermal conductivity (W/mK)
l	channel length upstream of the expansion section (m)
L	channel length downstream of the expansion section (m)
S	step height (m)
T	temperature (K)
Tb	bulk temperature, $Tb = 1/(A \times Ubar) \int T \times u\,dA$ (K)
T_{in}	temperature at the inlet section (K)
T_w	temperature at the wall (K)
$Ubar$	mean velocity, $Ubar = 1/A \int u\,dA$ (m/s)
u_i, u_j	velocity components (m/s)
u_{in}	velocity at the inlet section (m/s)
W	channel width (m)
x_i, x_j	Cartesian coordinates

Greek letters

ρ	specific mass (kg m^{-3})
μ	dynamic viscosity (N s m^{-2})
η	apparent viscosity (N s m^{-2})
$\bar{\eta}$	average apparent viscosity, $\bar{\eta} = 1/A \int \eta dA$ (N s m^{-2})
$\dot{\gamma}$	equivalent shear rate (s^{-1})

Subscripts

i, j	indexes
in	inlet
w	wall

pressure variations in 2D expansion flows and sensitivity analysis to the model parameters were presented by Zdanski and Vaz Jr. [11]. Temperature-dependent Cross and Power-Law Modified Arrhenius models were used to describe the non-Newtonian flow behaviour.

Three-dimensional expansion flows of polymer melts described by the generalized Newtonian model have received little attention. To the authors' best knowledge, the thermal effects on 3D expansion flows accounting for the viscous heating phenomenon have not been fully explained. Contrastingly, the literature shows increasing interest on 3D simulation of Newtonian flows. A range of physical aspects has been addressed for Newtonian flows based on numerical and experimental works in recent years. Armaly et al. [12] and Nie and Armaly [13,14] performed both experimental and numerical studies on 3D expansion flows, from which important hydrodynamic features were explored, such as the x_u-*line* definition and its dependence on the Reynolds number (see Section 3.2 for further details). Saldana et al. [15] analysed numerically heat transfer aspects of laminar flow of air in 3D expansions, where which some issues related to the Nusselt number distribution were addressed. More recently, Casarsa and Giannattasio [16] presented experimental PIV (Particle Image Velocimetry) results for turbulent mean flow of air in 3D expansions. The authors reported results for mean velocities and turbulent fluctuations and presented a comprehensive discussion on the 3D mean flow topology based on the analysis of streamlines at different 2D planes.

Measurement of local flow parameters, such as velocity and temperature distributions, in polymer melt flow is virtually impossible with the current technology. Therefore, understanding and analysis of the physics of the flow rely mostly on numerical simulation. In this sense, the present work discusses physical aspects of polymer melt flow in 3D sudden expansions. The flow topology (streamlines) and property distributions (temperature and viscosity) are addressed. The numerical scheme is based on central second order accurate finite difference formulae. The capability of the computational scheme to handle 2D non-Newtonian flows has been previously demonstrated in Vaz Jr. and Zdanski [8] and Zdanski and Vaz Jr. [17,18]. The validation (and verification) for solving 3D flows is also reported in the present study. The main results comprise streamlines and property contours (temperature and viscosity), indicating the presence of a highly three-dimensional vortical structure at the expansion section. As for Newtonian flows, such three-dimensional structure exhibits a complex spiral motion (backward to step and towards channel centre).

2. Theoretical formulation

2.1. Governing equations

Polymer melt flow in injection moulding can be described by the generalized Newtonian formulation. This approach solves the non-Newtonian flow by combining the same set of equations used for Newtonian flows and a nonlinear constitutive relation for viscosities (apparent viscosity). The latter describes the behaviour of a particular polymer as function of the shear strain rate and temperature. This strategy is largely used when stress relaxation and elastic effects in the polymer melts are negligible. The numerical formulation and discretization scheme contemplate only a steady-state flow condition. The mass, momentum and energy conservation laws for laminar flow, written in conservation law form, are given by

$$\frac{\partial u_i}{\partial x_i} = 0, \tag{1}$$

$$\frac{\partial(\rho u_i)}{\partial t} + \frac{\partial(\rho u_j u_i)}{\partial x_j} = -\frac{\partial p}{\partial x_i} + \frac{\partial}{\partial x_j}\left[\eta(T,\dot{\gamma})\left(\frac{\partial u_i}{\partial x_j} + \frac{\partial u_j}{\partial x_i}\right)\right], \tag{2}$$

$$\frac{\partial(\rho c T)}{\partial t} + \frac{\partial(\rho c u_i T)}{\partial x_i} = \frac{\partial}{\partial x_i}\left(k\frac{\partial T}{\partial x_i}\right) + \eta(T,\dot{\gamma})\dot{\gamma}^2, \tag{3}$$

where $i, j = 1,\ldots,3$ represent indicial notation and η is the apparent viscosity. The last term of Eq. (3) models the viscous heating effect, i.e., the conversion of mechanical energy into heat due to intrinsic friction within the flow. The Cross model is adopted for computing the apparent viscosity,

$$\eta(T,\dot{\gamma}) = \frac{\eta_0(T)}{1 + [\lambda(T)\dot{\gamma}]^{1-n(T)}}, \tag{4}$$

where

$$\eta_0(T) = a_1 \exp\left(\frac{a_2}{T}\right), \quad \lambda(T) = b_1 \exp\left(\frac{b_2}{T}\right) \quad \text{and}$$

$$n(T) = c_1 \exp\left(-\frac{c_2}{T}\right). \tag{5}$$

Pedro Bom et al. [19] adopt the following set of values: $a_1 = 0.022603$ Pa s, $a_2 = 5003.01$ K, $b_1 = 1.6425 \times 10^{-6}$ s, $b_2 = 3901.0$ K, $c_1 = 1.3574$, $c_2 = 653.73$ K. Furthermore, for this specific polymer, the thermo-physical properties used in the simulations are specific mass ($\rho = 1143.9$ kg/m^3), thermal conductivity ($k = 0.31$ W/mK) and specific heat ($c = 2420.0$ J/kgK).

The preceding constitutive relation describes the behaviour of a commercial polymer Poliacetal POM-M90-44. The term $\dot{\gamma}$ in Eqs. (2)–(4), stands for the equivalent shear rate, and reads

$$\dot{\gamma} = \sqrt{\frac{1}{2}\left(\frac{\partial u_i}{\partial x_j} + \frac{\partial u_j}{\partial x_i}\right)^2}. \tag{6}$$

For validation purposes, the same set of equations are used to model viscous laminar incompressible Newtonian flows by assuming $\eta = \mu$ in Eqs. (1)–(3). The term μ is the classical dynamic viscosity and represents a macroscopic property of a particular Newtonian fluid. All the remaining symbols in the preceding expressions are completely standardized in literature and are given in the nomenclature.

2.2. Numerical modelling

The conservation laws presented in Eqs. (1)–(3) are non-linear and fully coupled, representing a set of five equations for the unknowns, i.e., three velocity components (u, v and w), temperature (T) and pressure (p). Velocities and temperatures are determined by the momentum and energy equations, respectively. Therefore, the continuity equation, that establishes null divergent for the velocity field, is transformed into an equation for pressure. This is the classical problem known in literature as pressure–velocity coupling, typically found when devising numerical strategies for solving incompressible flows. The method adopted in this work is an extension for 3D flows of the 2D formulation presented in Vaz Jr. and Zdanski [8], where a Poisson equation for pressure is solved to assure a divergence-free velocity field. In addition, central finite difference formulae were adopted to discretize both convective and diffusive terms of the governing equations. The variables are arranged in a collocated mesh, and artificial viscosity terms are added externally to control the odd–even decoupling problem. The time evolution is accomplished by the implicit Euler method combined with a pseudo-transient march, aiming at a steady-state solution. For the 2D approach, the reader is referred to reference [8] for further discussions on the computational methodology. Its extension to 3D flows will be discussed elsewhere in a forum dedicated to computational modelling. Notwithstanding, some comparative studies are provided in this work in order to ascertain credibility of the numerical results.

3. Results and discussions

3.1. Problem statement and boundary conditions

The present work aims at studying the non-Newtonian 3D flow in a plane channel with asymmetric sudden expansion. The geometry with its mains dimensions is depicted in Fig. 1. The origin of the Cartesian system is placed at the expansion section in the middle span. The computational domain extends $\ell = 3S$ upstream of the expansion section, where the plug flow is assumed, i.e., constant x-velocity, $u(x = -\ell) = u_{in}$, and null y- and z-velocity components. A uniform temperature is also imposed at the inlet plane, $T(x = -\ell) = T_{in}$. The pressure at the inlet section is extrapolated from inside points, where a linear variation is assumed. The channel length downstream of the expansion section is assumed $L = 40S$. This distance ensures that exit boundary conditions (non-reflexive null derivative for all variables) do not affect numerical results. The expansion ratio of the channel ($ER = H/h$) is assumed equal to 2, being the channel thickness upstream and downstream of the expansion section $h = 2$ mm and $H = 4$ mm, respectively. The aspect ratio of the channel ($AR = W/S$) is assumed equal to 4. The channel positions $y = S$ (upstream of the expansion), $y = 0$ (downstream of the step), $y = H$ and $z = \pm W/2$ comprise solid walls. The boundary conditions at the walls correspond to non-slip for velocities, known values for temperatures (T_w) and null derivatives for pressure.

The computational mesh adopted in the simulations is non-uniform in the x-direction, with point clustering near the expansion section. The maximum stretching factor used is around 4%. In the y- and z-directions the mesh size is uniform. The region upstream of the expansion section ($-\ell \leqslant x \leqslant 0$, $S \leqslant y \leqslant H$, $-W/2 \leqslant z \leqslant W/2$) is mapped by $21 \times 31 \times 101$ grid points, whilst the downstream region ($0 \leqslant x \leqslant L$, $0 \leqslant y \leqslant H$, $-W/2 \leqslant z \leqslant W/2$) is divided into $101 \times 61 \times 101$ nodes. The full computational domain comprises 688,012 grid points.

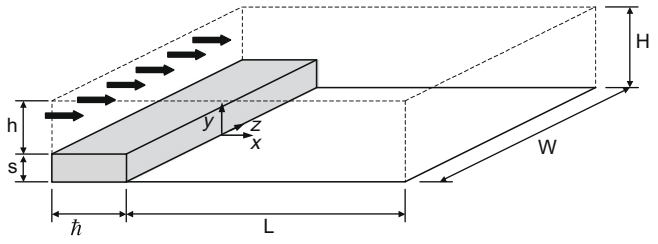

Fig. 1. Geometry representation with its main dimensions.

3.2. Validation and verification

The process of comparing a given numerical solution against experimental data is known in literature as validation. Otherwise, if a numerical solution is confronted against theoretical results, the procedure is generally referred as verification [20]. Therefore, the verification/validation process using benchmark problems is important for credibility of a numerical solution. The numerical scheme adopted in the present analysis was extensively tested in authors' previous works dealing with non-Newtonian 2D problems

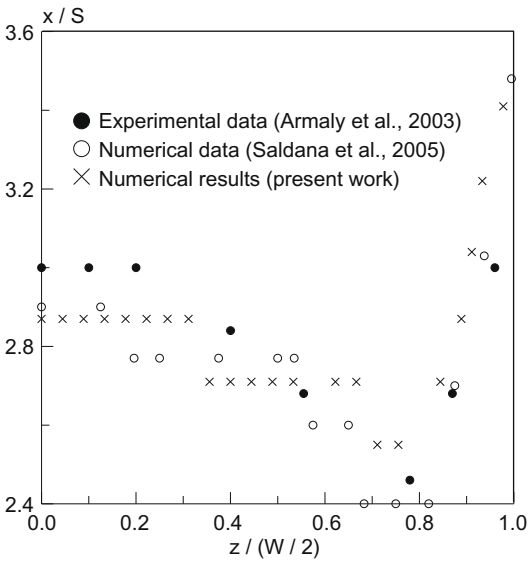

Fig. 2. X_u-line distribution along the spanwise direction.

[8,11,17,18]. This section presents a 3D validation/verification aiming at showing the capability of the scheme to handle this class of flow.

Experimental information, especially local velocities and temperatures, regarding polymer melts is scarce or even non-existent in the literature. Therefore, for validation of the numerical scheme, the Newtonian flow of air in a 3D expansion was considered. This flow geometry was studied by Armaly et al. [12], who reported experimental results for the laminar regime. The same geometry was also simulated recently by Saldana et al. [15]. Comparisons of the solutions are presented in Fig. 2 for a Reynolds number, $Re = (2\rho u_{in} S)/\mu = 98.5$. The physical parameter chosen is the x_u-*line* distribution along the spanwise direction. According to Armaly et al. [12], the x_u-*line* is the location on the stepped wall ($y = 0$) where the streamwise component of the wall shear stress $[\mu(\partial u/\partial y)_{y=0}]$ is equal to zero. This position is identified by locating along the x axis the region where the streamwise velocity component (u) changes sign from negative to positive (i.e. $u = 0.0$) at the closest parallel plane to the stepped wall ($y = 0$). Following Saldana et al. [15], the location is taken at the first node along the streamwise direction where the x-velocity component changes sign to positive. This procedure is normally used to identify the reattachment length for 2D separated flows. In addition, a close agreement of such parameter indicates also agreement of the flow recirculation topology and velocity distributions in the critical regions. Noticeably, the x_u-*line* presents variations in the spanwise direction due to the high three-dimensionality of the flow close the step. This feature can be identified in Fig. 2, which shows the results provided by Refs. [12,15] and the present work. It has been found that, from the channel centre ($z/(W/2) = 0.0$), there is a smooth decrease of x_u-*line* to a local minimum around position $z/(W/2) = \pm 0.75$, followed by a sharp increase near the lateral channel walls ($z/(W/2) = \pm 1.00$). The overall agreement of the present solution with Refs. [12,15] is satisfactory, being the differences mainly credit to two aspects: (i) the experimental data from Armaly et al. [12] and the numerical results of Saldana et al. [15] indicate the inlet velocity at different locations. The former does not inform the location where the boundary condition is imposed; it is mentioned only that the experiments yield a fully developed profile at the expansion session (at $x = 0$ in Fig. 2) without giving further details on the actual velocity distribution values. In Ref. [15], a fully developed profile is imposed at the channel entrance (at $x = -\ell$ in Fig. 2). The present solution adopts a uniform velocity distribution at the channel entrance ($u = u_{in}$, $v = 0$, $w = 0$) at $x = -\ell$; (ii) the numerical solution of Saldana et al. [15] is based on the SIMPLER algorithm [21], which is a first order upwind scheme, whereas the present solution is obtained using a second order accurate finite difference scheme [8].

The second test for verification purposes compares the present 3D non-isothermal, non-Newtonian scheme to solutions obtained using 2D finite elements for fully developed flows. The physical problem constitutes a polymer melt flow in a long duct with a square section $W = H$. The apparent viscosity is defined by the Cross constitutive relation (see Eqs. (4) and (5)). The present method solves the 3D flow entry problem with velocity and temperature distributions reaching fully developed conditions towards the exit section. The finite element approximation is based on a 2D fully developed flow model (see [22] for further details on the numerical description) and provides solutions for velocities and temperatures for the fully developed flow section. The main results are presented in Fig. 3 for non-dimensional velocity and temperature profiles along the z-axis at $y = H/2$. It has been observed that the agreement between both numerical solutions is quite satisfactory for velocities and temperatures. Differences between non-dimensional solutions are also presented in Fig. 3. In both cases, the largest differences are found close to the walls and at the channel centre, distributed in a symmetrical pattern.

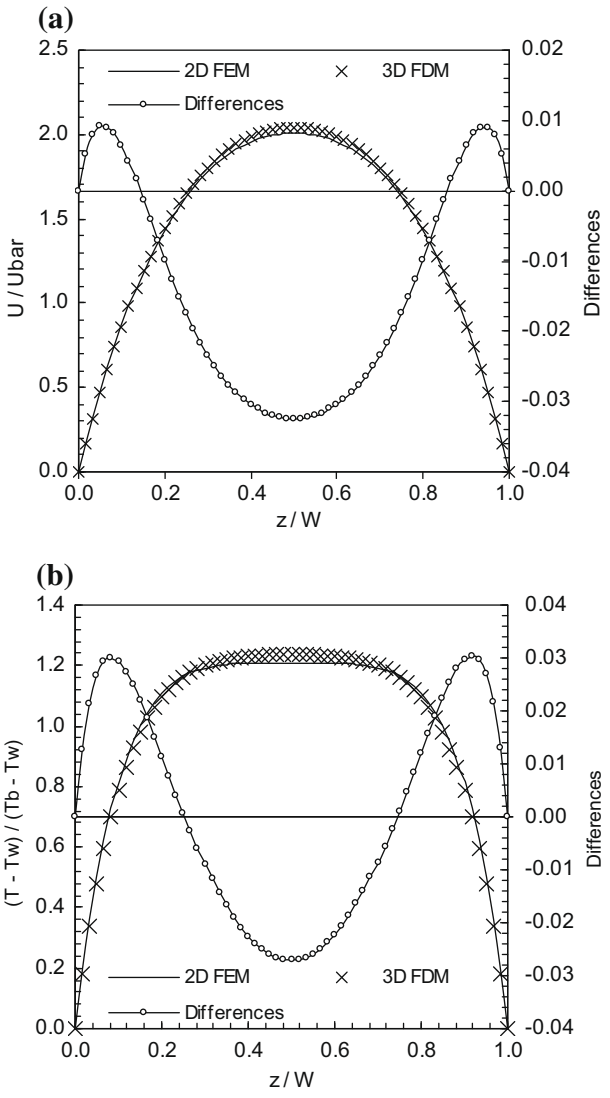

Fig. 3. Non-dimensional temperature and streamwise velocity: 2D finite element solution (FEM) vs. 3D finite difference solution (FDM) along the channel centre line ($y = H/2$) for fully developed flow.

3.3. Physical analysis

The fluid viscosity exhibited by polymer melts is exceedingly higher than common Newtonian fluids such as air, water or oil.

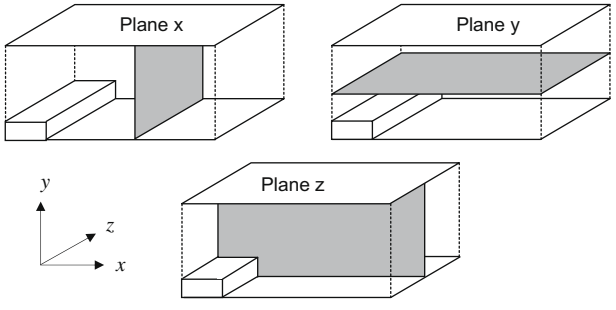

Fig. 4. 2D planes intercepting x, y and z axes.

Therefore, the characteristic Reynolds number of the problem is typically low, ranging around 10^{-4}–10^{-3} [17,18], thereby favouring a laminar flow regime. The velocities (and flow rates) prescribed at the inlet channel section correspond to values normally used in industrial injection problems. The present work aims at studying the basic physical features of the polymer flow without loosing the practical aspect of the problem. The results and discussions presented in this section comprise the flow topology (streamlines are computed by the projection of the velocity field in given 2D planes), property distributions (temperature and viscosity contour plots) and x_u-*line* and x_w-*line* variations along the spanwise direction. The 2D planes along *x*, y and *z* directions are represented in Fig. 4, where the nomenclature is defined. The analysis is restricted to the region close to the expansion section where the flow is highly three-dimensional.

According to Armaly et al. [12], for 3D laminar Newtonian flows, the x_u-*line* depends upon the Reynolds number. Aiming at assessing such findings for polymer melts, the x_u-*line* distribution is presented in Fig. 5. In this case, location of $u = 0$ is determined by a linear interpolation between positions of the closest nodes to the sign change of the u velocity component. The results comprise two inlet velocities u_{in} = 6 cm/s and 12 cm/s, which correspond to Reynolds numbers, $Re = (\rho u_{in} S)/\bar{\eta} = 1.3 \times 10^{-4}$ and 3.0×10^{-4}, respectively. The temperature boundary conditions at the solid walls and inlet section are $T_w = T_{in}$ = 453.0 K. The term $\bar{\eta}$ is the average apparent viscosity evaluated at the channel exit section ($x = L$). It is interesting to mention that such definition is used in an attempt to better capture the shear rate and viscous effect (which in turn affect the Reynolds number). The average apparent viscosity is, therefore, computed at a given cross-section, which, in the present case, corresponds to the channel exit section (where the flow variables reach nearly fully developed conditions). The results of Fig. 5 reveal that the x_u-*line* for polymer melts presents similar tendency to Newtonian flows, i.e., from the channel centre ($z/(W/2) = 0.00$) there is a smooth decrease to a local minimum around $z/(W/2) = \pm 0.72$, followed by a sharp increase in the vicinity of the lateral channel walls ($z/(W/2) = \pm 1.00$). Otherwise, the influence of the Reynolds number is moderate, being felt only in the core region around the middle span.

Aiming at a better understanding the physics of the flow, the x_w-*line* distribution is presented also in Fig. 5. The x_w-*line* is the locus close to the stepped wall ($y = 0$) where the spanwise component of wall shear stress is zero, e.g., $\mu(\partial w/\partial y)_{y=0}$. This point is identified by observing the position along *z* direction where the *w*-velocity component changes sign (i.e. $w = 0$). Furthermore, the position where the x_u-*line* intercepts x_w-*line* defines the region where the equivalent wall shear stress is null [15]. The results of Fig. 5 show that, for the present polymer rheology and flow rates, this point is located around $x/S = 0.29$ and $z/(W/2.0) = \pm 0.90$. More details and new physical insights relating to this point will be provided further in the text.

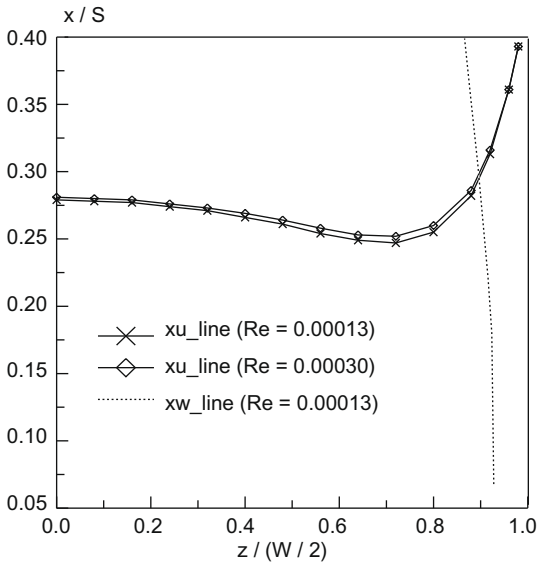

Fig. 5. X_u-line and x_w-line distributions along the spanwise direction.

Streamline maps, temperature and viscosity contours at selected 2D planes in *x*, y and *z* directions are reported in Figs. 6–12, from which the physics of the flow near the step (expansion section) is discussed. Due to their 3D nature, streamlines shown in Figs. 6–8 are computed from the projection of the velocity field in different locations on the *x*–*y*, *x*–*z* and *y*–*z* planes. The velocity and temperature boundary conditions for this simulation corresponds to u_{in} = 6 cm/s, $T_{in} = T_w$ = 453.0 K. Since the wall and inlet temperatures are the same, any temperature increase in the domain is due only to flow friction (viscous heating effect).

The 3D flow topology is discussed by analysing the 2D planes in *x*, y and *z* directions indicated in Fig. 4. Firstly, streamlines for *x*–*y* planes are presented in Fig. 6. The three planes in the spanwise direction (*z*1, *z*2 and *z*3) show the flow topology from the step ($x/S = 0$) until a section taken around $x/S = 2.2$. It is relevant to mention that, in the plane at the middle span (*z*1), the flow topology is qualitatively similar to the 2D expansion flows [7,8]. A confined vortex is detected in the concave corner with dimensions around $x/S = 0.28$ and $y/S = 0.32$. The same flow topology is found for the *z*2 plane ($z/S = 1.0$), in which a small reduction of the vortex dimensions is observed. Finally, for the *z*3 plane, the physical picture is drastically changed: near the lateral wall ($z/S = \pm 1.92$), no vortex zone can be detected in the 2D *x*–*y* plane. The flow in this plane is upstream (*u* negative) from $x/S = 0$ (step) until around $x/S = 0.32$. The *z*3 plane is placed in the region where the three-dimensional effects are more relevant. The positions $x/S = 0$, $y/S = 0$ and $z/S = \pm 2$ correspond to the interception of three walls defining a three dimensional concave corner.

The streamlines at *x*–*z* sections are presented in Fig. 7 for planes *y*1, *y*2 and *y*3. The section *y*1 corresponds to $y/S = 0.03$, i.e., the first computational point away from the stepped wall ($y/S = 0.0$). This particular plane intercepts the recirculation zone found at the *x*–*y* sections, and helps to clarify important aspects about the 3D flow topology. (i) Firstly, the flow symmetry around $z/S = 0$ (middle span): this aspect evinces that the numerical solution converged to a possible physical solution, since at such low Reynolds number no flow bifurcation takes place. (ii) The region of reverse flow in the *x*-direction (*u* negative) is clearly detected along the spanwise direction. It is worth noting that the line along *z* direction where streamlines emerge (see Fig. 7) corresponds exactly to the x_u-*line* plotted in Fig. 5. In this region, the flow is highly three-dimensional, i.e., *u* is negative and *w* is found to be deflected from lateral walls and pulled towards the channel centre. Therefore, the fluid particles in this recirculation zone present a spiral motion. (iii) Finally, there is a particular position in this plane (the nearest plane to the stepped wall) where the equivalent wall shear stress is null (*u* and *w* velocity components are zero). From analysis of Fig. 5, this point is located around $x/S = 0.29$ and $z/(W/2.0) = \pm 0.90$ (position where the x_u-*line* intercepts the x_w-*line*). In the *x*–*y* plane represented in Fig. 7a, these positions can be easily located at $x/S = 0.29$ and $z/S = \pm 1.8$. Therefore, such analysis provides key insights on the 3D flow behaviour in the vicinity of the stepped wall: the locations where $u = w = 0.0$ are the only regions in the *y*1 plane where the velocity vector points downward and is normal to the stepped wall, i.e, these positions mean the origin of all streamlines (as observed in Fig. 7).

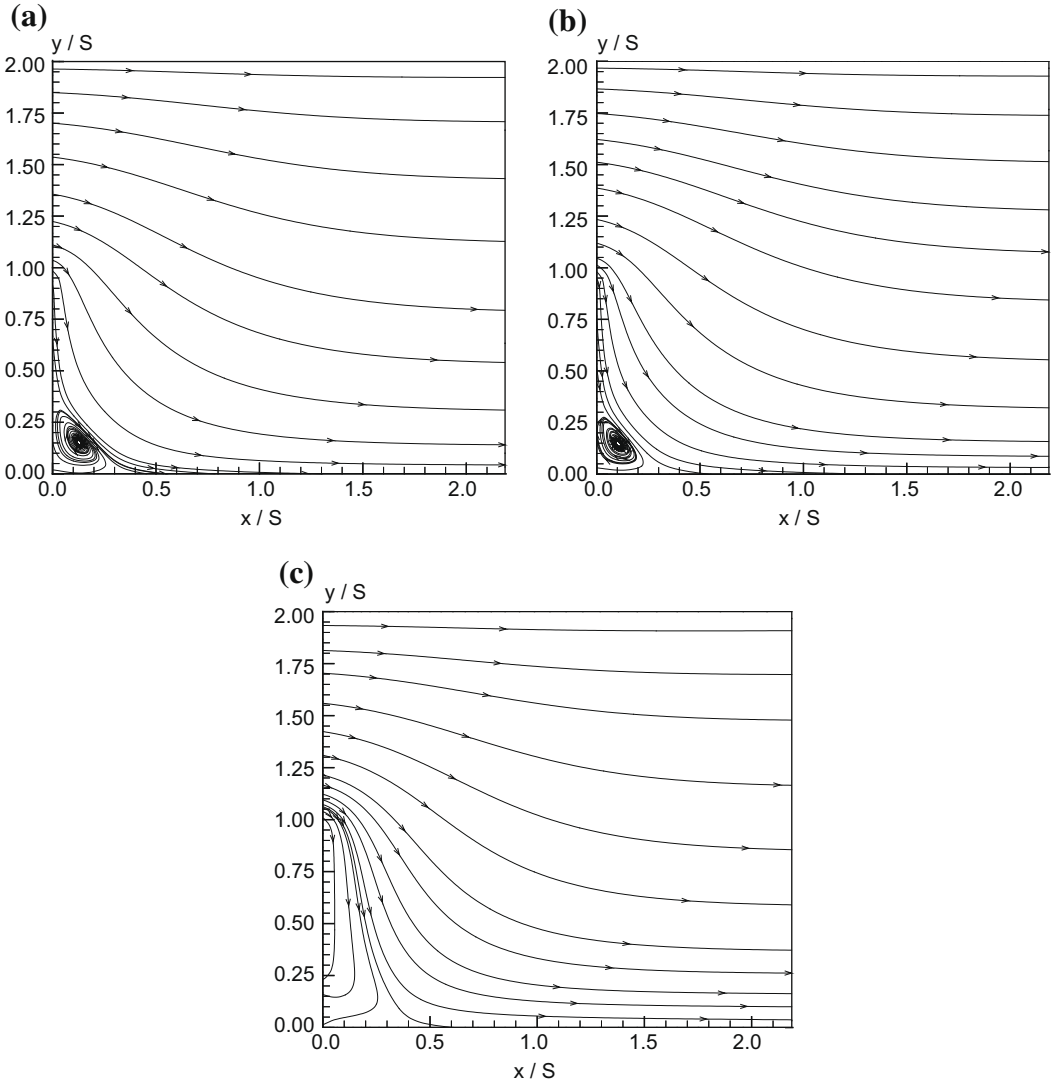

Fig. 6. Streamlines for x–y planes: (a) plane $z1$ – middle span ($z/S = 0$), (b) plane $z2$ – intermediate region ($z/S = \pm 1$) and (c) plane $z3$ – close to the lateral walls ($z/S = \pm 1.92$).

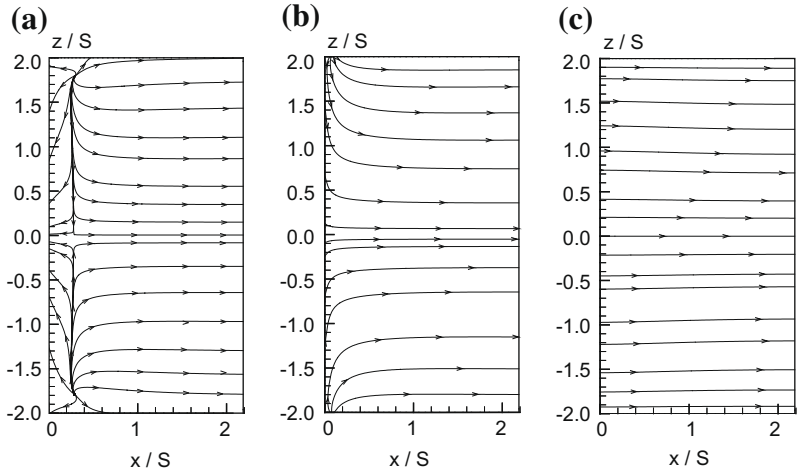

Fig. 7. Streamlines for x–z planes: (a) plane $y1$ – close to the stepped wall ($y/S = 0.03$), (b) plane $y2$ – middle step ($y/S = 0.5$) and (c) plane $y3$ – flow core ($y/S = 1.5$).

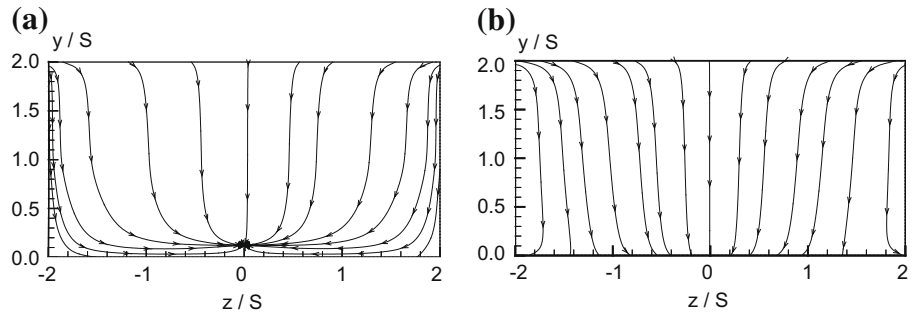

Fig. 8. Streamlines for z–y planes: (a) plane $x1$ – close to the step ($x/S = 0.14$) and (b) plane $x2$ – at location $x/S = 0.92$.

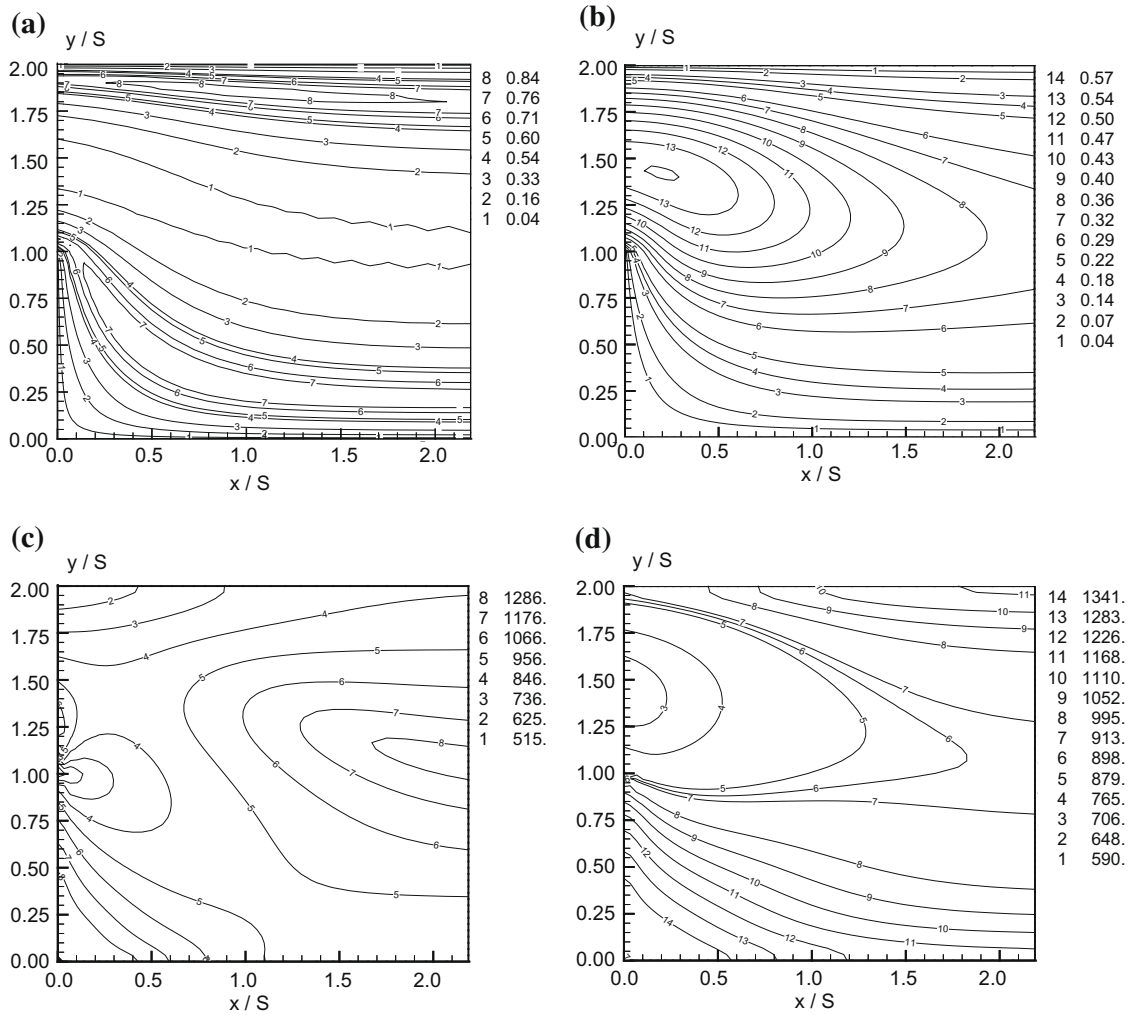

Fig. 9. Temperature increment [K] and viscosity [Pa s] for x–y planes: (a) temperature and (c) viscosity for plane $z1$ – middle span ($z/S = 0$); (b) temperature and (d) viscosity for plane $z3$ – close to the lateral walls ($z/S = \pm 1.92$).

The streamlines for planes $y2$ and $y3$ are also presented in Figs. 7b and 7c: (i) The section $y2$ corresponds to $y/S = 0.5$ and shows that, near expansion section ($0.0 < x/S < 0.5$), the flow is deflected from lateral walls towards the channel centre. Further along the downstream direction ($x/S > 0.5$), the streamlines become nearly parallel to the lateral walls (the w velocity component is very small). No recirculation zone is observed in the $y2$ plane. (ii) The plane $y3$ corresponds to a position $y/S = 1.5$ and shows a region where the flow is basically along the x direction (w velocity component is very small).

Fig. 8 shows the streamlines for z–y planes, namely $x1$ ($x/S = 0.14$) and $x2$ ($x/S = 0.92$). The attention is focused on the step section since v and w velocity components decrease sharply to nearly zero around a position $x/S = 1.5$. (i) The $x1$ plane intercepts the recirculation zone observed in Figs. 6 and 7, showing a downward flow towards the stepped wall (v negative) and deflected

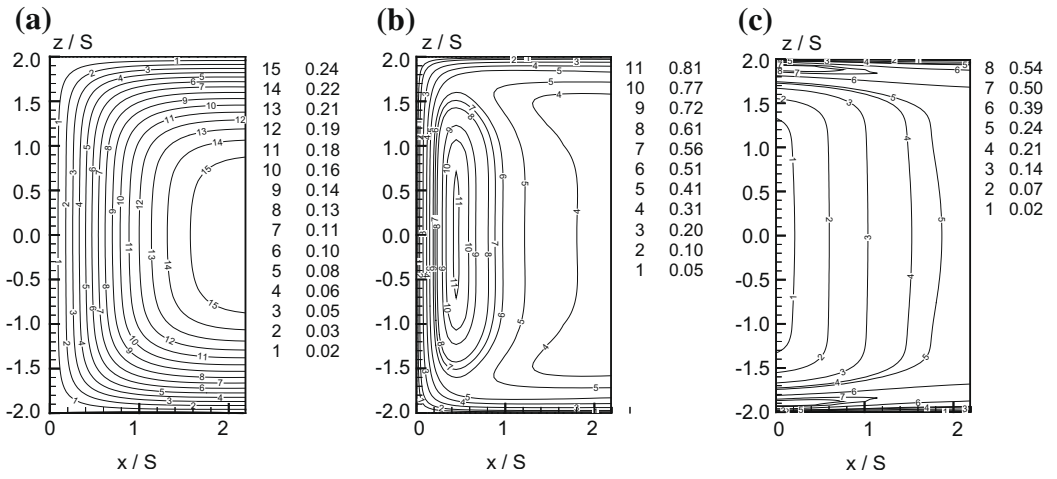

Fig. 10. Temperature increment [K] for x–z planes: (a) plane $y1$ – close to the stepped wall ($y/S = 0.03$), (b) plane $y2$ – middle step ($y/S = 0.5$) and (c) plane $y3$ – flow core ($y/S = 1.5$).

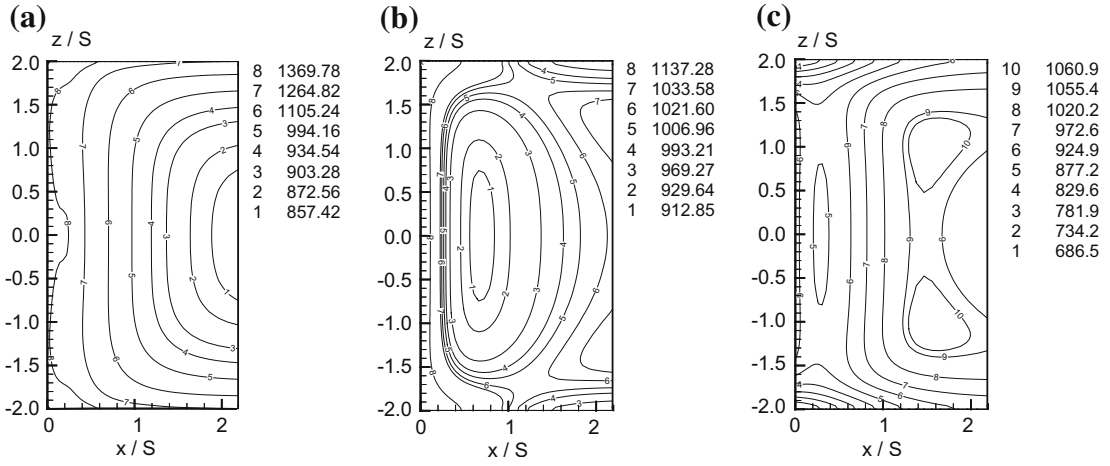

Fig. 11. Viscosity [Pa s] for x–z planes: (a) plane $y1$ – close to the stepped wall ($y/S = 0.03$), (b) plane $y2$ – middle step ($y/S = 0.5$) and (c) plane $y3$ – flow core ($y/S = 1.5$).

from lateral walls to the channel centre. All streamlines merge to a point at the middle span located at $z/S = 0.0$ and $y/S = 0.13$. It is interesting to observe in Fig. 6 that the point on the $z1$ plane placed at $x/S = 0.14$ and $y/S = 0.13$ represents the centre of the recirculation zone. (ii) The plane $x2$ is placed further in the downstream direction and shows a distinct pattern close to the lateral and stepped walls ($y/S = 0.0$ and $z/S = \pm 2.0$); The w velocity component in this region is in opposite direction, i.e., the flow is deflected towards the lateral walls the same conclusion may be drawn from observing Fig. 7a for the $y1$ plane.

Remark. Based on the discussions of the preceding paragraphs for distinct 2D planes (Figs. 6–8), a realistic picture of the 3D flow topology may be constructed. (i) The flow topology is highly three-dimensional only close to the expansion section ($0.0 < x/S < 1.5$). (ii) In addition, only one recirculation region is identified, as observed in Figs. 6 and 7 for $z1$, $z2$ and $y1$ planes. This vortex structure resembles a spiral, being well defined from the middle span region ($z/S = 0.0$) up to $z/S = \pm 1.80$. (iii) In the regions near the lateral and stepped walls the w velocity component presents opposite behaviour (see Fig. 8 for planes $x1$ and $x2$). In the vortex region, due to the spiral motion, the fluid particles are pulled down towards the channel centre, whilst a little further downstream the fluid particles are pushed towards the lateral walls. In spite of this change in flow direction, no well-defined recirculation region was detected near the lateral walls, as shown in Figs. 7 and 8.

The temperature distributions for x–y planes $z1$ and $z3$ are presented in Fig. 9. The figure shows temperature increments relative to the wall temperature, $\Delta T = T(x,y,z) - T_w$, i.e., the temperature increment is due to the viscous heating effect since $T_{in} = T_w$ is assumed in this example. In the plane $z1$ ($z/S = 0.0$), the maximum temperature rise takes place near the upper wall ($y/S \approx 1.8$) and in the region further downstream of the convex corner ($x/S = 0.0$ and $y/S = 1.0$). The flow topology in these regions shows streamlines highly deflected (see Fig. 6), indicating significant velocity gradients, which in turn, produces higher shear rates. Despite the smaller absolute differences, the temperature distribution for $z3$ plane is drastically changed, since this section is placed at the neighbourhood of a lateral wall ($z/S = \pm 1.92$). The maximum temperature increment in the $z3$ plane is found near the step around the point $x/S = 0.2$ and $y/S = 1.5$. It is interesting to observe that, in the $z1$ plane, this position presents exactly the minimum temperature rise. Clearly, the location $y/S = 1.5$ on the $z3$ plane corresponds to a region where the flow is pushed from the lateral walls towards the channel centre due to the spiral motion effect in the vortex zone. Otherwise, at the same position on the $z1$ plane, the flow is nearly two-dimensional with lower shear rates [8,11].

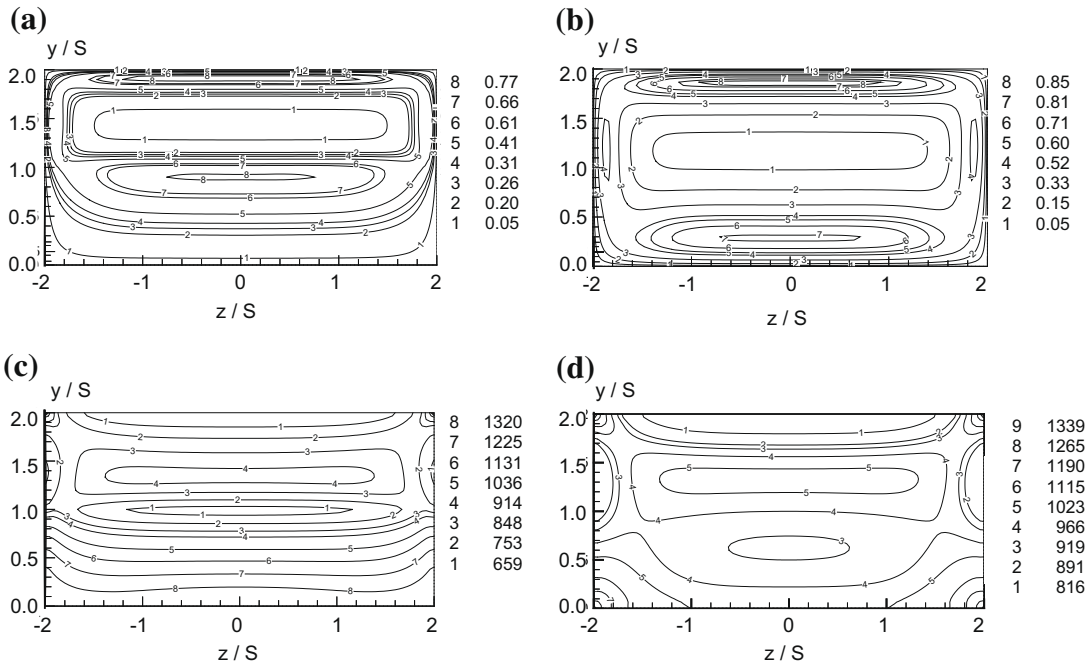

Fig. 12. Temperature increment [K] and viscosity [Pa s] for z–y planes: (a) temperature and (c) viscosity for plane $x1$ – close to the step ($x/S = 0.14$); (b) temperature and (d) viscosity for plane $x2$ – at location $x/S = 0.92$.

The contour levels for viscosities are also presented in Fig. 9 for $z1$ and $z3$ planes. In spite of the strong temperature dependency (see Eqs. (4) and (5)), for the present flow rate and channel geometry, viscosity variations are dominated by the equivalent shear rate, i.e., at a given inlet/wall temperature, the small viscous heating leads to an also small temperature increase (temperature increase in these planes is less than 1.0 K). The maximum values of viscosity on the $z1$ plane are found near the channel centre and concave corner, whereas, for the $z3$ plane, the maximum viscosity is found near the concave corner. Both regions present low shear rates. Notwithstanding, the polymer flow presents huge viscosity variations (a markedly non-Newtonian behaviour) in all regions of the problem domain.

Fig. 10 presents temperature contour levels for x–z planes $y1$, $y2$ and $y3$, from which symmetry about the middle span plane ($z/S = 0$) can be observed. Firstly, the maximum temperature rise due to viscous heating effect occurs at the $y2$ plane, near the middle span. This section ($y/S = 0.5$) intercepts the region with higher temperature increment captured also on the $z1$ plane ($z/S = 0.0$). The plane $y1$, however, intercepts the region near the stepped wall with low velocities. The temperatures for this section exhibit a continuous increase from the lateral walls and step towards the channel centre at middle span ($z/S = 0.0$). The viscous heating effect at $y1$ plane is less pronounced. Finally, the $y3$ plane intercepts a region where the flow is nearly uniform at its core. The maximum temperature rise in this plane takes place near the lateral walls close to the expansion section (the region where the shear rate is higher). This region can be easily identified in Fig. 9b for the $z3$ plane at the neighbourhood of $y/S = 1.5$. The viscosity contours for the same x–z planes are plotted in Fig. 11. For plane $y1$, the viscosity distribution is exactly opposed to the temperature behaviour (see Figs. 10a and 11a): the minimum values for viscosities are found in the region of maximum temperature increments. Both $y2$ and $y3$ planes intercept regions of higher shear rate, and, consequently, lower viscosities.

Fig. 12 presents temperature and viscosity contours for z–y planes. The $x1$ plane intercepts the region near expansion section ($x/S = 0.14$) and clearly shows that the core region (around $y/S = 1.5$) is little affected by the viscous heating. However, the regions at the middle span ($z/S = 0.0$), near the step ($y/S < 1.0$) and upper wall ($y/S = 2.0$), present larger temperature increments due to the high curvature of the streamlines (see Fig. 6 for $z1$ plane). Further in the downstream direction, for $x2$ plane ($x/S = 0.92$), the temperature distribution is almost symmetric about z- and y-axes, i.e., maximum temperature rise near the four solid walls in the regions of higher shear rates. This is an indication that the flow is evolving towards a fully developed condition. When the fully developed flow is reached, the maximum temperatures are at the channel centre and the polymer flow is said to attain the equilibrium regime, i.e., all heat generated due to viscous heating is transferred transversally to the solid walls [17,18]. In addition to temperatures, Fig. 12 presents also viscosity distributions. Viscosities at the $x1$ plane ($x/S = 0.14$) are generally smaller then those at the $x2$ plane ($x/S = 0.92$) due to the higher shear rate (larger velocity variations) near the step. Viscosity distribution at the $x2$ plane reflects the tendency of the flow to follow the topology of a rectangular channel: large viscosities at the corners and channel core (due to smaller shear rates).

4. Concluding remarks

Three dimensional, steady state polymer melt flow in sudden expansion was investigated using a computational scheme based on finite differences. Validation and verification were performed by comparing, respectively, experimental data for Newtonian flow in a similar channel, and numerical results for a fully developed polymer melt flow in a rectangular channel.

The 3D flow topology was discussed based on 2D streamlines maps for x, y and z directions. The main findings are as follows: (i) The flow is highly three-dimensional only close to the expansion section ($0.0 < x/S < 1.5$). (ii) Only one recirculation zone, resembling a spiral, is identified (see Figs. 6 and 7 for $z1$, $z2$ and $y1$ planes), being well-defined from the middle span region ($z/S = 0.0$) up to $z/S = \pm 1.80$. (iii) In this vortex region, due to the spiral motion,

the fluid particles are pulled down towards the channel centre, whilst a little further downstream, the fluid particles are pushed towards the lateral walls. In spite of this change in flow direction (w velocity component changes sign), no well-defined recirculation region was detected near the lateral walls (Figs. 7 and 8).

Despite the strong influence of the inlet and wall temperatures on viscosities, the effect of temperature rise due to viscous heating is rather limited in the present case (the maximum temperature rise is less then 1.0 K, being most evident in regions of deflected streamlines – or higher shear rates). On the other hand, the temperature solution, given by Eq. (3), is essential to provide a general framework to solve the problem for different inlet temperatures or even when mould and inlet temperature are different. Otherwise, the large viscosity variation within the problem domain evinces the strong non-Newtonian behaviour of the polymer melt, being dominated by the shear rate and directly affected by the velocity gradient.

Acknowledgments

This work was partially supported by FAPESC (Santa Catarina Foundation for Scientific and Technological Research), under Grant 12508/2007-3. The second author also acknowledges the scholarship provided by CNPq (National Council for Scientific and Technological Development, Project – PQ – 309147/2006-9).

References

[1] P. Neofytou, D. Drikakis, Non-Newtonian flow instability in a channel with a sudden expansion, J. Non-Newtonian Fluid Mech. 111 (2003) 127–150.
[2] R. Mânica, A.L. De Bortoli, Simulation of sudden expansion flow for Power–Law fluids, J. Non-Newtonian Fluid Mech. 121 (2004) 35–40.
[3] P. Ternik, J. Marn, Z. Zunik, Non-Newtonian fluid flow through a planar symmetric expansion: shear-thickening fluids, J. Non-Newtonian Fluid Mech. 135 (2006) 136–148.
[4] P. Neofytou, Transition to asymmetry of generalised Newtonian fluid flows through a symmetric sudden expansion, J. Non-Newtonian Fluid Mech. 133 (2006) 132–140.
[5] F.P. Pinho, P.J. Oliveira, J.P. Miranda, Pressure losses in the laminar flow of shear-thinning Power-Law fluids across a sudden axe–symmetric expansion, Int. J. Heat Fluid Flow 24 (2003) 747–761.
[6] D.M. Binding, P.M. Phillips, T.N. Phillips, Contraction/expansion flows: the pressure drop and related issues, J. Non-Newtonian Fluid Mech. 137 (2006) 31–38.
[7] W. Bao, An economical finite element approximation of generalized Newtonian flows, Comput. Methods Appl. Mech. Eng. 191 (2003) 3637–3648.
[8] M. Vaz Jr., P.S.B. Zdanski, A fully implicit finite difference scheme for velocity and temperature coupled solutions of polymer melt flow, Commun. Numer. Methods Eng. 23 (2007) 285–294.
[9] S.C. Chen, K.F. Hsu, Numerical simulation and experimental verification of melt front advancements in co-injection molding process, Numer. Heat Transfer A: Appl. 28 (1995) 503–513.
[10] A. Wachs, J.R. Clermont, A. Khalifeh, Computations of non-isothermal viscous and viscoelastic flows in abrupt contractions using a finite volume method, Eng. Comput. 19 (8) (2002) 874–901.
[11] P.S.B. Zdanski, M. Vaz Jr., Non-isothermal polymer melt flow in sudden expansions, J. Non-Newtonian Fluid Mech. (in revision) (2008).
[12] B.F. Armaly, A. Li, J.H. Nie, Measurements in three-dimensional laminar separated flow, Int. J. Heat Mass Transfer 46 (2003) 3573–3582.
[13] J.H. Nie, B.F. Armaly, Three-dimensional convective flow adjacent to backward-facing step – effects of step height, Int. J. Heat Mass Transfer 45 (2002) 2431–2438.
[14] J.H. Nie, B.F. Armaly, Reattachment of three-dimensional flow adjacent to backward-facing step, ASME J. Heat Transfer 125 (2003) 422–428.
[15] J.G. Barbosa Saldana, N.K. Anand, V. Sarin, Forced convection over three-dimensional horizontal backward facing step, Int. J. Comput. Methods Eng. Sci. Mech. 6 (2005) 225–234.
[16] L. Casarsa, P. Giannattasio, Three-dimensional features of the turbulent flow through a planar sudden expansion, Phys. Fluids 20 (2008) 015103 1–015103 15.
[17] P.S.B. Zdanski, M. Vaz Jr., Polymer melt flow in plane channels: effects of viscous dissipation and axial heat conduction, Numer. Heat Transfer A – Appl. 49 (2006) 159–174.
[18] P.S.B. Zdanski, M. Vaz Jr., Polymer melt flow in plane channels: hydrodynamic and thermal boundary layers, J. Mater. Process. Technol. 179 (2006) 207–211.
[19] R. Pedro Bom, M.H. Herrmann, H. Soares Hoays, Rheological analysis via flow simulator (in Portuguese), in: SULMAT 2000, Joinville – Brazil, 2000, 948–957.
[20] W.L. Oberkampf, T.G. Trucano, Verification and validation in computational fluid dynamics, Progress Aerospace Sci. 38 (2002) 209–272. 2002.
[21] S.V. Patankar, Numerical Heat Transfer and Fluid Flow, Hemisphere Publishing Corporation, Washington, 1980. pp. 131–134.
[22] M. Vaz Jr., E.L. Gaertner, Finite element and finite volume simulation and error assessment of polymer melt flow in closed channels, Commun. Numer. Methods Eng. 22 (2006) 1077–1085.